ChemComm

COMMUNICATION

View Article Online
View Journal | View Issue

Cite this: *Chem. Commun.*, 2024, **60**, 8553

Received 24th June 2024,
Accepted 8th July 2024

DOI: 10.1039/d4cc03071k

rsc.li/chemcomm

Geometrically twisted intra–inter-molecular cooperative interactions for an enhanced photo-response in an ORMOSIL-based host–guest system†

Moumita Chandra, Alpana Sahu, Nitul Kalita and Mohammad Qureshi *

In situ **encapsulation of the 2-(2′-hydroxylphenyl)benzothiazole (HBT) fluorophore into organically modified silica (ORMOSIL) is recognized as a potential approach to increase the photocurrent conversion efficiency. Encapsulation resulted in a twisted geometrical configuration of HBT with an efficient charge transfer and increased carrier density, resulting in a 246% photo-response enhancement.**

In the field of photo-electrochemistry, the design and development of photoactive materials have emerged as a crucial research task due to their wide applications in photocatalysis, photovoltaics, and sensing.[1,2] Photoactive materials serve as transducers that convert electrochemical energy to chemical energy in the presence of solar light.[3]

There has been great interest in structurally diverse organic fluorescent materials due to their ability to be customized through chemical modifications, which results in extending their large-scale applications in photovoltaic cells, light-emitting diodes and fluorescent probes.[4] Among these, the fluorophore HBT is notable for its well-studied photosensitivity, photostability and bioimaging driven by intramolecular hydrogen bonding responsible for facilitating the excited-state intramolecular proton transfer (ESIPT) process, where a hydrogen bond donor and hydrogen bond acceptor co-exist in a single molecule.[5,6] However, the fluorescence properties of HBT could suffer from self-absorption and strong intramolecular interactions primarily due to ESIPT and intrinsic radiative decay.[7]

To overcome these limitations, various research groups have focused on fine-tuning the fluorophore material by blocking the ESIPT process and enhancing fluorophore performance by incorporating various functional groups. A recent emerging approach consists of an HBT fluorophore moiety embedded within functionalized silica, enabling significant performance enhancement.[8] This strategy offers several advantages, such as mitigating charge recombination, enhancing stability and expanding the range of applications through synergistic interactions between the fluorophore and host material. This composite design has the potential to unlock new possibilities in fluorescence-based technologies by combining the unique properties of fluorophores with those of other materials.

Silica nanoparticles are one of the most preferred materials due to their non-toxicity, thermal stability, chemical inertness, and biocompatibility.[9] However, silica nanoparticles lack a high surface area and are unsuitable for guest–host interactions. Therefore, the use of organic precursors such as alkyl-substituted silicon alkoxides introduces performance-enhancement properties inside inorganic silane, and this modified material is known as organically modified silica (ORMOSIL).[10]

The covalent bonding between organic and inorganic components in ORMOSIL creates a cross-linked organic porous network viable for host–guest interactions.[11] There are numerous applications for this modified form in bioimaging, gas sensing, lasers, and many others. Palmisano *et al.* reported a TiO_2/ORMOSIL thin film doped with phthalocyanine dyes for the application of photocatalytic devices under solar light irradiation.[12] ORMOSIL acted as a host-cage material, and when phthalocyanine dyes were incorporated inside the cage, large improvements were subsequently observed in the performance. Mishra *et al.* reported carbon nanodots incorporated inside ORMOSIL for the fabrication of fluorescent coatings on glass.[13] Therefore, chemical modification of ORMOSIL matrices can effectively replace traditional materials, particularly in the field of photochemistry.

In this context, encapsulating HBT into an ORMOSIL matrix offers significant advantages to chronoamperometry applications in the presence of light. However, to the best of our knowledge, there are no reports describing the fabrication of HBT on an ORMOSIL matrix employed for photoresponse purposes. Herein, we propose a convenient one-pot synthesis for creating an HBT–ORMOSIL composite for photocurrent measurements, where intermolecular charge transfer occurs instead of ESIPT by virtue of the twisted geometry of HBT, which promotes the intermolecular charge transfer, as described in Scheme 1. We

Materials Science Laboratory, Department of Chemistry, Indian Institute of Technology Guwahati, Guwahati, India. E-mail: mq@iitg.ac.in

† Electronic supplementary information (ESI) available: Experimental section, FESEM, EDX, FT-IR, XRD, UV-DRS, photocurrent study, TRPL, Mott–Schottky, and NMR analysis. See DOI: https://doi.org/10.1039/d4cc03071k

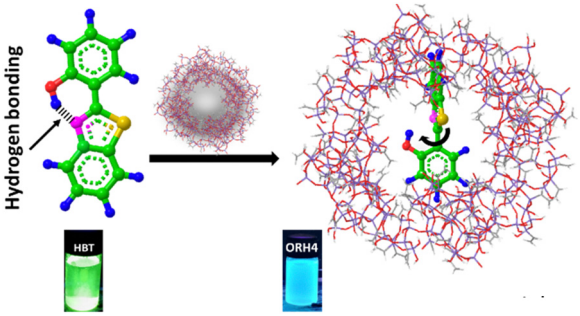

Scheme 1 Schematic representation of the interactions between HBT and ORMOSIL, which is a host–guest system. The digital photograph of HBT under ultraviolet radiation and the composite show the incorporation of HBT in the ORMOSIL matrix, with the wavelength blue-shifted in the composite.

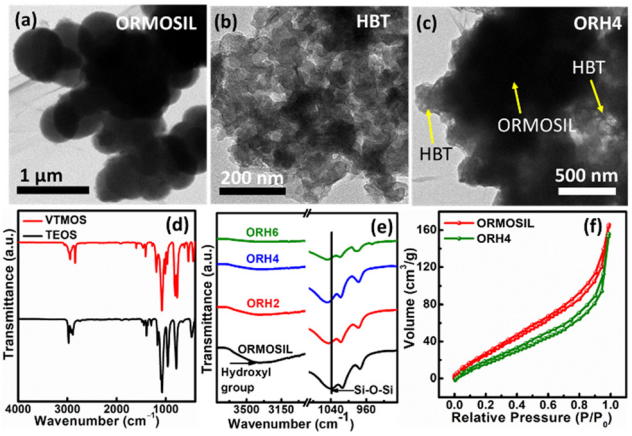

Fig. 1 FETEM images of (a) ORMOSIL, (b) HBT and (c) ORH4; FT-IR spectra of (d) TEOS and VTMOS, and (e) the synthesized materials in the stretching frequency region of Si–O–Si and the hydroxyl group. (f) N_2 adsorption–desorption isotherm of ORMOSIL and ORH4 shows that after incorporation of HBT in ORMOSIL, the surface area decreased.

conducted extensive studies to demonstrate the inhibition of ESIPT, and the introduction of the intermolecular charge transfer within the HBT–ORMOSIL framework served as the driving force for enhancing the photo-current response.

ORMOSIL was synthesized *via* the hydrolysis–condensation method[14] (the detailed experimental procedure is given in the ESI†), where tetraethyl orthosilicate (TEOS) is mixed with vinyl trimethoxy silane (VTMOS), followed by hydrolysis and condensation using NaOH. The condensation reaction proceeds, and ORMOSIL is formed, which was confirmed by physico-chemical characterizations. The obtained thick white-coloured liquid was further stirred for 1 h and further dried in an oven at 60 °C for 12 h. The synthesis process of the composite is the same, with the addition of HBT before hydrolysis to trap HBT inside the ORMOSIL-caged framework. The hydrolysis and condensation reaction mechanisms of the precursors for the formation of ORMOSIL are explained in the ESI.†[14] Various compositions of ORMOSIL-HBT composite were synthesized by varying the amount of HBT, and composites were designated as ORH2 (2 mmol HBT), ORH4 (4 mmol HBT), and ORH6 (6 mmol HBT). A diagram of the interactions between HBT and ORMOSIL is shown in Scheme 1.

Field emission transmission electron microscopy (FETEM) analysis was carried out for the detection of microstructure, and Fig. 1a shows the spherical morphology of ORMOSIL, with HBT showing a relatively smaller morphological structure (Fig. 1b). The FETEM image of the ORH4 composite in Fig. 1c depicts the interconnected network structure of the composite, with HBT uniformly distributed throughout the ORMOSIL matrix. This interconnected structure is advantageous for enhancing the efficiency of charge transfers *via* the caged network. To determine the elemental distribution within the material, energy-dispersive X-ray (EDX) analysis was conducted, and it was found that all elements were homogeneously distributed in the composite (Fig. S2, ESI†).

Fourier transform-infrared (FT-IR) spectroscopy is an essential tool for effectively identifying functional groups within the material. There were typical peaks for TEOS between 2975 and 2880 cm^{-1}, representing the C–H stretching vibration of the ester group (Fig. 1d and Fig. S3a, ESI†), whereas the peaks between 1443 and 1296 cm^{-1} were related to the asymmetric bending or wagging of C–H bonds.[15] The peaks at around 1167 and 968 cm^{-1} corresponded to C–H rocking. The Si atom bound to the ethoxy group ($Si–OCH_2CH_3$) is represented by the peaks at around 1100 cm^{-1}. In VTMOS (Fig. 1d and Fig. S3a, ESI†), the spectra recorded at 1078 cm^{-1} and 1188 cm^{-1} were attributed to the methoxy group, whereas the vinyl group appeared at 1008 cm^{-1} and 966 cm^{-1}.[16]

After the formation of ORMOSIL, the most prominent absorption peak appearing at 1037 cm^{-1} corresponded to the asymmetric stretching of the Si–O–Si bonds, and the peak at 758 cm^{-1} was due to the Si–O stretching vibration, which implies the hydrolysis of TEOS and VTMOS under basic conditions and successful synthesis of ORMOSIL (Fig. 1e and Fig. S3b, ESI†).[17–19] The weak signal at 966 cm^{-1} was attributed to the overlap of signals arising from Si–OH stretching and vinyl CH_2 wagging. The band for the bending vibration of the surface-adsorbed hydroxyl group appears at 3368 cm^{-1}. The characteristic bands of HBT are shown in Fig. S3b (ESI†). After the formation of the composite, the FT-IR spectra showed the characteristic bands of ORMOSIL and HBT. However, a shift in the Si–O–Si stretching vibration was observed for the composites, as shown in Fig. 1e, which implies intermolecular interactions between HBT and ORMOSIL instead of a new chemical bond formation. The peak corresponding to the hydroxyl group in ORMOSIL broadened, and the peak intensity decreased, as shown in Fig. 1e, indicating the interaction of hydroxyl groups in the composite.

The nuclear magnetic resonance (NMR) study of HBT and ORH4 revealed that intramolecular hydrogen bonding in HBT was disrupted in the composite as the intensity of the OH proton diminished, and the peak position shifted in the composite as discussed in later stages. Therefore, the FT-IR and NMR analyses indicate that HBT and ORMOSIL are attached in a single framework. Moreover, encapsulation of HBT in the ORMOSIL matrix was further validated from a Brunauer–Emmett–Teller (BET) isotherm, as shown in Fig. 1f.

Pure ORMOSIL shows a higher BET surface area of 137 $m^2\ g^{-1}$ as compared to ORH4 (104 $m^2\ g^{-1}$). A decreased value in the BET surface area indicated that a network structure resulted when HBT was incorporated inside the porous matrix of ORMOSIL due to a decrease in the surface area of the composite as compared to pure ORMOSIL.

HBT emits in the green light region *via* its enol–keto form, which occurs through ESIPT, where intramolecular hydrogen bonding facilitates the tautomerization to the keto form.[20] Well-resolved UV absorption spectra of pure HBT exhibit a maximum absorbance in the range of 380 nm (Fig. S4, ESI†). After the formation of composite, the absorbance shifted towards the lower wavelength region (339 nm for ORH4), as indicated by the arrow mark in the normalized absorption spectra in Fig. S4b (ESI†). Intramolecular hydrogen bonding is responsible for the ESIPT process because the proton transfer takes place between the phenyl group and N-atom of the benzothiazole ring of HBT. However, the intermolecular interactions between HBT and the Si–OH group in the ORMOSIL framework impedes the ESIPT process and results in geometrical twisting of HBT, which is the key factor for the charge transfer in the HBT–ORMOSIL composite.

Additionally, in photoluminescence (PL) spectra (Fig. 2a), the emission of ORH4 is blue-shifted to 450 nm, as compared with the emission at 510 nm for pure HBT and indicates changes in the neighbouring environment involving HBT in the excited state, resulting in facile charge transfers in the composite.[21] The emission colour changing from green to blue (as shown in the digital photograph in Scheme 1) indicates the inhibition of the ESIPT process,[22–24] where the HBT molecule is trapped inside the ORMOSIL matrix through intermolecular interaction.

To further investigate the charge transfer dynamics of synthesized materials, time-resolved photoluminescence (TRPL) analysis was carried out and is shown in Fig. 2b. TRPL decay was fitted with a bi-exponential decay model according to the following equation:[25]

$$I = A_1 e^{t/\tau_1} + A_2 e^{t/\tau_2} \quad (1)$$

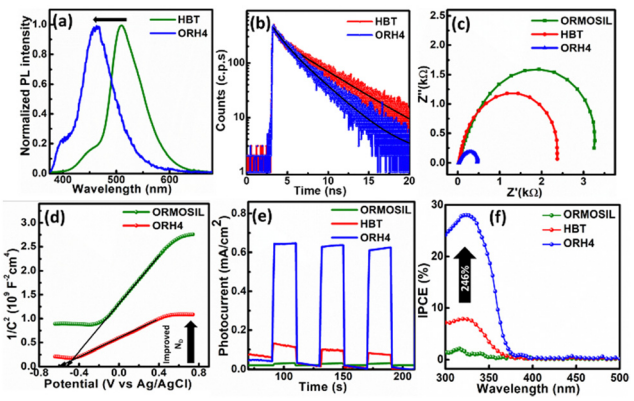

Fig. 2 (a) Steady-state photoluminescence spectra indicate that the emission wavelength was blue-shifted after the formation of the HBT–ORMOSIL composite. (b) TRPL plot, (c) EIS spectra, (d) Mott–Schottky plot, (e) photocurrent measurements and (f) IPCE study of the materials.

where I represents the normalized PL intensity, A_1 and A_2 represent the component percentage, and τ_1 indicates faster and τ_2 represents slower lifetime components of the respective excited state species. In the literature, it has been shown that these two components are usually assigned to molecular emission and emission resulting from charge transfer processes.[26] The charge transfer process usually occurs faster than its molecular emission counterpart, resulting in a faster average lifetime of the species in the emission profile. The faster τ_2 of the ORH4 sample (3.18 ns) compared to the HBT sample (4.6 ns) suggests more efficient photogenerated charge separation through the composite.[27] This observation is supported by the PEC performance, where the composites exhibited superior performance compared to HBT.

Electrochemical impedance spectroscopy (EIS) analysis also validated the charge transfer mechanism in ORH4, as given by the smaller semicircle in the EIS analysis (Fig. 2c). Mott–Schottky measurements were carried out to further elucidate carrier concentrations (N_D). As shown in Fig. 2d, ORH4 gives a smaller slope in the Mott–Schottky plot as compared to pure ORMOSIL, which indicates higher carrier concentration in the composite (the details appear in the ESI†).

The chronoamperometry analysis was carried out using as-synthesized catalysts in a solution of 0.5 M Na_2SO_4 under 1 Sun illumination at 20 s chopping interval. A fast photocurrent response was observed, and the highest photocurrent density of 0.65 mA cm^{-2} was obtained from ORH4 as compared to ORH2 and ORH6, as shown in Fig. S5 (ESI†) at a fixed potential 0.7 V (*vs.* Ag/AgCl), which is 21 and 5 times greater than ORMOSIL and HBT, respectively, as shown in Fig. 2e. There was a significant decrease in photocurrent anodic spikes for ORH4 as compared to pure materials, indicating that the charge recombination was suppressed, and the photocurrent response was stable for the composite. To quantify the efficiency, incident photon-to-current conversion efficiency (IPCE) measurements were carried out and are shown in Fig. 2f. The photoconversion efficiency of ORH4 increased by ~246% as compared to HBT. The enhancement in IPCE is related to the reduced recombination of charge carriers by virtue of the intermolecular interactions between HBT and ORMOSIL.

NMR spectroscopy analysis was carried out to elucidate the inherent twisted molecular geometry involved in governing the charge transfers between caged molecules. Fig. S6a (ESI†) shows the NMR spectra of pure HBT. The peaks in the range of δ = 6.5 to 8.5 ppm were attributed to protons attached to the aromatic ring (Ar–H) and are seen as singlet, doublet, doublet–doublet and triplet peaks.[8] The singlet peak observed at δ = 11.55 ppm was attributed to the (–OH) proton, which is due to the intramolecular hydrogen bonding between the phenolic proton and nitrogen atom of the thiazole ring.[28]

After the formation of the HBT–ORMOSIL matrix, a significant reduction in the singlet peak intensity corresponding to –OH, as well as peak shifting towards the de-shielded region, was observed (Fig. S6b, ESI†). This indicated the disruption of intramolecular hydrogen bonding in HBT and the intermolecular interactions in the caged structure of the ORMOSIL

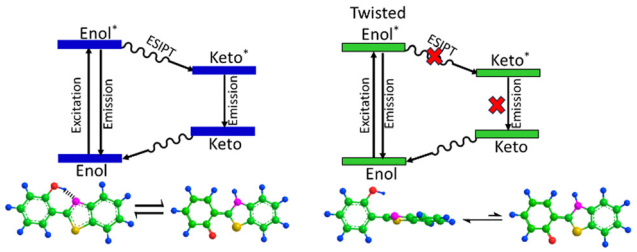

Fig. 3 ESIPT in HBT and inhibition of the ESIPT process in the presence of ORMOSIL in the caged framework are shown.

matrix with the –OH group of HBT. Additionally, a significant shift in the NMR spectra of the aromatic region implies that the interaction of HBT with the ORMOSIL matrix in the composite and benzothiazole ring occurred in a different chemical environment in the composite (Fig. S6c and d, ESI†).

In the FT-IR spectra, we observed a shift in the Si–O–Si stretching vibration towards a higher wavenumber region, which is indicative of guest–host interactions of HBT and the ORMOSIL matrix. Furthermore, the peak intensity at 3368 cm^{-1} of the hydroxyl group in the composite decreased and broadened. The NMR study also indicates peak shifting of HBT, and changes in the neighbouring environment around it established the intermolecular interactions between HBT and the ORMOSIL matrix. Fig. 3 shows the inhibition of the ESIPT process in HBT in the presence of the ORMOSIL matrix. Additionally, the Mott–Schottky analysis provided an estimate of carrier concentration in the materials, which elucidated the higher carrier concentration in the composite (ORH4), and the charge transfers from HBT to ORMOSIL increased the photocurrent response in the caged ORMOSIL-HBT matrix under illumination.

In summary, this work showcases host–guest interactions between HBT and ORMOSIL, where a fluorophore embedded within an organically modified silica matrix results in heightened photocurrent performance. Host–guest type interactions lead to geometry twisting, which results in effective charge transfers and subsequent photo-current response.

M. C. contributed to the ideation, experiments, data analysis, and drafting of the manuscript. M. Q. contributed the initial ideation, manuscript writing and supervised the overall work and funding. A. S. and N. K. contributed equally to the analysis and manuscript writing.

M. C. acknowledges IIT Guwahati for the Institute Post-Doctoral Fellowship. Anjana Singha is acknowledged for BET measurements. M. Q. thanks DST-SERB for financial support through project no: SERB/CRG/2020/00211. The authors are thankful to the Department of Chemistry and Central Instruments Facility (CIF) at IIT Guwahati for the instrumental support.

Data availability

The data supporting this article have been included as a part of the ESI.† and the instruments used in the experiments were mentioned in the experimental section.

Conflicts of interest

There are no conflicts to declare.

References

1 Y. Peng, C. H. Mak, J.-J. Kai, M. Du, L. Ji, M. Yuan, X. Zou, H.-H. Shen, S. P. Santoso, J. C. Colmenares and H.-Y. Hsu, *J. Mater. Chem. A*, 2021, **9**, 26628–26649.
2 K. Yan, P. K. Kannan, D. Doonyapisut, K. Wu, C. Chung and J. Zhang, *Adv. Funct. Mater.*, 2021, **31**, 2008227.
3 J. Lv, J. Xie, A. G. A. Mohamed, X. Zhang and Y. Wang, *Chem. Soc. Rev.*, 2022, **51**, 1511–1528.
4 Z. Wang, Q. Jingjing, X. Wang, Z. Zhang, Y. Chen, X. Huang and W. Huang, *Chem. Soc. Rev.*, 2018, **47**, 6128–6174.
5 S. Pijeau, D. Foster and E. G. Hohenstein, *J. Phys. Chem. B*, 2017, **121**, 4595–4605.
6 P. Majumdar and J. Zhao, *J. Phys. Chem. B*, 2015, **119**, 2384–2394.
7 A. C. Sedgwick, L. Wu, H.-H. Han, S. D. Bull, X.-P. He, T. D. James, J. L. Sessler, B. Z. Tang, H. Tian and J. Yoon, *Chem. Soc. Rev.*, 2018, **47**, 8842–8880.
8 M. Güçoğlu and N. Şatıroğlu, *J. Mol. Liq.*, 2022, **348**, 118388.
9 A. A. Nayl, A. I. Abd-Elhamid, A. A. Aly and S. Bräse, *RSC Adv.*, 2022, **12**, 13706–13726.
10 S. Dash, S. Mishra, S. Patel and B. K. Mishra, *Adv. Colloid Interface Sci.*, 2008, **140**, 77–94.
11 F. Selvestrel, *et al.*, *Nanoscale*, 2013, **5**, 6106–6116.
12 G. Palmisano, M. C. Gutiérrez, M. L. Ferrer, M. D. Gil-Luna, V. Augugliaro, S. Yurdakal and M. Pagliaro, *J. Phys. Chem. C*, 2008, **112**, 2667–2670.
13 M. K. Mishra, A. Chakravarty, K. Bhowmik and G. De, *J. Mater. Chem. C*, 2015, **3**, 714–719.
14 M. Pagliaro, R. Ciriminna, M. W. C. Man and S. Campestrini, *J. Phys. Chem. B*, 2006, **110**, 1976–1988.
15 A. Hadela, M. Lakić, M. Potočnik, A. Košak, A. Gutmaher and A. Lobnik, *Adsorpt. Sci. Technol.*, 2020, **38**, 168.
16 S. S. Abbas, G. J. Rees, N. L. Kelly, C. E. J. Dancer, J. V. Hanna and T. McNally, *Nanoscale*, 2018, **10**, 16231–16242.
17 T. K. Sahu, S. Arora, A. Banik, P. K. Iyer and M. Qureshi, *ACS Sustainable Chem. Eng.*, 2017, **5**, 5912–5921.
18 C. Odenwald and G. Kickelbick, *J. Sol-Gel Sci. Technol.*, 2019, **89**, 343–353.
19 X. Zhang, W. Lin, J. Zheng, Y. Sun, B. Xia, L. Yan and B. Jiang, *J. Phys. Chem. C*, 2018, **122**, 596–603.
20 V. S. Padalkar and S. Seki, *Chem. Soc. Rev.*, 2016, **45**, 169–202.
21 Y. Ren, L. Zhou and X. Li, *Front. Chem.*, 2021, **9**, 807433.
22 I. Kaur, R. Shivani, P. Kaur and K. Singh, *Dyes Pigm.*, 2020, **176**, 108198.
23 X. Yang, R. Lu, H. Zhou, P. Xue, F. Wang, P. Chen and Y. Zhao, *J. Colloid Interface Sci.*, 2009, **339**, 527–532.
24 Z. Wu, J. Dou, K.-U. Nguyen, J. C. Eppley, K. Siwawannapong, Y. Zhang and J. S. Lindsey, *Molecules*, 2022, **27**, 8682.
25 T. R. Chetia, D. Barpuzary and M. Qureshi, *Phys. Chem. Chem. Phys.*, 2014, **16**, 9625–9633.
26 M. J. Mayoral, P. Ovejero, M. Cano and G. Orellana, *Dalton Trans.*, 2011, **40**, 377–383.
27 W. Yang, S. Lee, H. C. Kwon, J. Tan, H. Lee, J. Park, Y. Oh, H. Choi and J. Moon, *ACS Nano*, 2018, **12**, 11088–11097.
28 S. Sahana, G. Mishra, S. Sivakumar and P. K. Bharadwaj, *Dalton Trans.*, 2015, **44**, 20139–20146.